Effects of non-thermal plasma treatment on the geopolymerization of kaolin clay

Berthelot SOP-TAMO
Universite de Ngaoundere
Jean Baptiste TARKWA
Universite de Ngaoundere
Thamer Alomayri
Umm Al-Qura University
HASAN ASSAEDI
Umm Al-Qura University
Jean Paul KAMSEU MOGO
Institute of Agricultural Research for Development
Jean Baenla
University of Yaounde I: Universite de Yaounde I
Georges KAMGANG-YOUBI
University of Yaounde I: Universite de Yaounde I
Leonel Tchadjié Noumbissié (leoneltchadjie@yahoo.com)
University of Johannesburg https://orcid.org/0000-0002-3778-3040

Research Article

Keywords: kaolin, activation, gliding arc plasma, geopolymerization process, compressive strength

Posted Date: February 12th, 2021

DOI: https://doi.org/10.21203/rs.3.rs-218862/v1

Version of Record: A version of this preprint was published at Silicon on May 12th, 2021. See the published version at https://doi.org/10.1007/s12633-021-01134-z.

Abstract

Cameroonian kaolin samples were used to produce geopolymer cements. Prior to its application, the raw kaolin samples were activated trough the gliding arc plasma treatment in both spatial post-discharge and direct mode. A mixture of sodium hydroxide and silicate was used as the alkaline solution. The materials produced were tested by X-ray diffraction, thermogravimetric analysis, differential scanning calorimeter and Fourier transform infrared spectroscopy in order to study the influence of the modifications generated by the gliding arc plasma treatment on the geopolymerization process. The scanning electron microscopy analyses, nitrogen physisorption analyses and compression tests were also carried out on the materials produced for assessing and understanding their mechanical performance. The results showed that the geopolymerization process remained partial at the curing temperature of 90 °C. Plasma spatial post-discharge mode treated kaolin led to 20.48% increase in compressive strength when compared with the geopolymer prepared from raw kaolin.

1 Introduction

In many field activities and in particular civil engineering, binders, and especially cements are of great interest because they form with water or with an alkaline solution, a plastic paste capable of agglomerating by hardening various substances. The manufacture of hydraulic cements considered as ordinary cements requires high energy consumption [1]. Moreover, the cement production leads to 5–8% of CO_2 global emissions and therefore constitutes a major drawback from an environmental point of view [2].

Literature review demonstrated that geopolymer cements can be used as an alternative to ordinary Portland cements in order to reduce CO_2 emissions [3, 4]. For instance, the optimal production of 1 metric ton of geopolymeric cement generates 0.180 metric ton of CO_2 from combustion of carbon-fuel, compared with 1 metric ton of CO_2 for Portland cement, that is, six times less [5]. Geopolymers are a class of semi-crystalline aluminosilicate materials, typically synthesized at room temperature or slightly elevated by a chemical reaction between an amorphous aluminosilicate powder and a highly concentrated alkaline solution [6–8]. The geopolymerization process is carried out in three phases, the first step consists in the dissolution of the aluminosilicate material for the formation of the reactive precursor ions $[SiO(OH)_3]^-$ and $[Al(OH)_4]^-$ [9].

This dissolution process depends on some characteristics of the aluminosilicate such as its hydrophilicity, chemical composition, mineralogy, surface area and especially on the material crystallinity. Accordingly, kaolinitic clays are calcined to be amorphised and therefore transformed into metakaolin before being used as an aluminosilicate material [10, 11]. However, the use of kaolin instead of metakaolin could be beneficial as it can avoid the high temperatures (500°-800 °C) calcination step. Furthermore, metakaolin derived geopolymers require too much water due to an increase of their porosity [12]. To enlighten, a development of low cost and sustainable strategies avoiding the use of thermal treatment is of great interest.

Recently, non-thermal plasma technologies withdrawn increasing interest for several applications such as surface treatment, textural properties modification, organic matter oxidation etc. Previous works demonstrated that the plasma treatment of kaolin improves its solubility whereas the material crystallinity was slightly modifying [13–16]. The physico-chemical modifications of activated kaolin particles could improve their geopolymeric reactivity. To our best knowledge, to date, no literature work has investigated the gliding arc plasma processing kaolin powder in the geopolymerization process. For all those reasons, this paper investigates the use of gliding arc plasma instead of the heat treatment. Gliding arc plasma pre-treatment of kaolin might contribute to the greener, less energy-consuming production of green concrete.

The objective of this article is to verify whether the modifications that occur during the gliding arc plasma treatment of kaolin are likely to significantly and positively influence the geopolymerization process and compressive strength of the materials obtained.

2 Experimental Study

2.1 Materials

Kaolin was used as the aluminosilicate raw material and was obtained from natural deposit in Cameroon. It was enriched in argillaceous mineralogical phase by wet sieving then; the dried clay was crushed and sieved with an 80 µm mesh sieve.

2.2 Plasma treatment of kaolin

The resulting raw kaolin labeled K was treated with gliding arc plasma for 30 min using moist air as feeding gas at the flow rate of 800L/h. Two methods of treatment were carried out: the direct treatment, where the target is exposed in contact with the highly primary reactive species generated in the plasma discharge and the spatial post-discharge treatment (indirect mode), in which the target (kaolin) is placed in another reactor (secondary reactor) where it interacts with long-live plasma-generated species flowing from the primary reactor [15]. The plasma treated kaolin sample in the direct mode was labeled K_1 and the plasma spatial post-discharge processed kaolin sample was labeled K_2.

2.3 Geopolymers synthesis

The alkaline activator solution was prepared by mixing 10M sodium hydroxide solution with the commercial sodium silicate solution. The proportion of sodium silicate was 7% of the mass of the sodium hydroxide solution. The resulting alkaline solution was sealed to prevent reaction with CO_2 from the atmosphere and then stored for at least 24 h at ambient temperature before use. The 24-hour storage was done to allow full silica dissolution, cooling and equilibration. The sodium water glass solution had a composition by weight of: 28.7% SiO_2, 8.9% Na_2O and 62.4% H_2O and the bulk density was 1400 kg/m^3.

The pastes were prepared as followed: the various kaolin samples (K, K_1 and K_2) were mixed with the alkaline solution for 10 min (4 min at slow speed and 6 min at high speed) in an M & O brand mixer, model N50-G. The powder/liquid activator mass ratio of 1.34 was used. The paste obtained was used for shaping the test specimens using cylindrical PVC molds (diameter of 20 mm and height of 40 mm). The specimens were labeled as follow: GP for the material produced with K, GP_1 for the material produced with K_1 and GP_2 for K_2. After casting, the specimens were vibrated for 3 min on an M&O brand electric vibrating table, type 202, No. 106 to expel air trapped by particulate matter during mixing.

Thereafter, the paste specimens were cured for 24 h at ambient temperature in the laboratory (30 ± 3 °C) then at 90 °C in an oven of the Heraeus VT 50.42 Ek brand for 24 h to accelerate the hardening. Demoulding was carried out after the previous operations and the samples were then stored at ambient temperature in a dry place for 28 days. To ensure reproducibility, six duplicate specimens were prepared for each geopolymer paste.

2.4 Analytical techniques

The chemical composition of the kaolin was determined using ICPAES (Inductive Coupled Plasma-Atomic Emission Spectrometry).

The powder diffractograms of the kaolin samples and of the materials produced were obtained on a Bragg-Brentano type apparatus (Bruker D8 advanced). This device is equipped with a Ge (111) monochromator operating by reflection of $K\alpha_1$ radiation from copper (λ = 1.54056Å); the scanned angular domain (2θ) is between 5 and 80°. Identification of crystalline phases was performed using ASTM files.

The FTIR analyses were carried out using a BRUKER alpha-p brand spectrometer with pure ethanol as solvent. The FTIR spectra were collected over a wave number range of 400 to 4000 cm^{-1}. The correction of the baselines of the obtained spectra was performed using the ATR algorithm incorporated in an FTIR software package named OPUS. A linear model was chosen. All FTIR analyses were carried out at room temperature.

Morphological characteristics at the micrometric scale were carried out by scanning electron microscopy, using a Philips FEI XL γ0 FEG ("Field Emission Gun") device.

To obtain information on the pores in the materials, BET analyses were performed with a micrometric analyser; Tristar 3000 model by nitrogen adsorption/desorption at 77°K. Each sample is first degassed at 423°K under vacuum for 1 h. The detection of open porosity is then done by injecting a nitrogen/helium stream in a 30/70 ratio. The BET equations were used.

Regarding the thermal analyses, an analyser of the brand LINSEIS model STA PT-1000 was used. Therefore, 20 mg of materials are introduced into the alumina crucible of a sample holder equipped with a precision balance. The heating rate is set at 10 °C/min under an air atmosphere (Self-Generated Atmosphere of Air).

The compressive strength was measured at the age of 28 days using a M&O brand electro-hydraulic press, type 11.50, No. 21. These tests were carried out according to EN 196-1 [17].

3 Results And Discussion

3.1 Characterization of raw and plasma modified kaolin samples

The chemical and mineralogical compositions of raw kaolin were reported in our previous work. From XRF analysis, the raw kaolin mainly consisted of silicon oxide (SiO_2), aluminum oxide (Al_2O_3), trace compounds such as Iron III oxide (Fe_2O_3), Titanium oxide (TiO_2) while the loss on ignition was 14.75%. However, the main mineral was kaolinite. There were other minor phases such as Quartz (Q), Gibbsite (G), Anatase (A), and Muscovite (M) in smaller proportions [15].

Some characteristics of plasma treated kaolin were also reported in our previous study. The gliding arc plasma is able to functionalize kaolinite contained in kaolin powder. Exposure of kaolin clay material to gliding arc plasma caused an overall increase in FTIR absorbance peaks of the clay material, such as lower bands around the values 1622 and 1391cm^{-1} due to the breakdown of certain Si–O–Si and Si–O–Al chemical bonds and the appearance of new peaks in the hydroxyl region (around the wave number values 3670 and 3520cm^{-1}). This corresponds to the formation of new hydroxyl groups on the surface of the material. Moreover, an increase in total dissolved solids for both direct and indirect treatment modes reflected the increase of the kaolin hydrophilicity [15].

Figure 1 gives the thermograms of the various kaolin samples. In general, DSC curves showed three endothermic phenomena and one exothermic phenomenon:

- the endothermic peak around 50°C corresponds to the removal of hygroscopic water;
- the second endothermic peak between 278 and 282°C is characteristic of gibbsite dehydroxylation according to equation 1:

$$2Al(OH)_3 \xrightarrow{278-282^{o}C} Al_2O_3 + 3H_2O \ ; \qquad (1)$$

- the third and most important endothermic peak, between 505 and 509°C revealed the dehydroxylation of kaolinite transforming into metakaolinite according to equation 2:

$$Si_2O_5Al_2(OH)_4 \xrightarrow{505-509^{o}C} 2SiO_2, Al_2O_3 + 2H_2O \ ; \qquad (2)$$

- the exothermic peak around 985°C is related to the structural reorganization of metakaolinite into spinel according to equation 3 [18]
- ;

$$2[2SiO_2, Al_2O_3] \xrightarrow{985^{o}C} Si_3Al_4O_{12} + SiO_2 \quad . \qquad (3)$$

Metakaolinite — spinelle

From the TGA curves, three thermal phenomena can be highlighted:

- a small mass loss between 20 and 250°C is related to the elimination of hygroscopic water;
- a significant mass loss between 250 and 450°C corresponding to the dehydroxylation of gibbsite;
- an important mass loss between 450 and 600°C corresponding to the dehydroxylation of kaolinite to metakaolinite.

It can be seen that the mass loss corresponding to the dehydroxylation of kaolinite was greater for K_1 (-8.33%) and K_2 (-9.68%) when compared with the sample K (-6.62%). This difference confirms the formation of new aluminol surface groups on the kaolinite after the plasma treatment of the kaolin powder. In addition, the previous observation suggests that the spatial post-discharge treatment mode is more appropriate for the functionalization of the kaolinite in comparison to the direct plasma treatment mode for this purpose.

3.2 Characterization of geopolymers

3.2.1 FTIR analysis

Figure 2a-d show infrared spectra of geopolymers obtained. Figure 2b-d are the zoomed-in of four interesting areas of Fig. 2a.

On the spectra of Fig. 2b, the bands at 3619 and 3690cm^{-1} corresponds to the elongation vibrations of the hydroxyl groups of kaolinite [19]; however, there was a sharp decrease in the intensity of these peaks (~70%). These observations indicate that the kaolinite particles were significantly dissolved by the alkaline solution but still remained in the system. The quantitative study of geopolymer's infrared spectra also revealed that, GP contains more kaolinite than GP_1 and GP_2. This suggests that the treatment improves the dissolution of kaolinite during the first step of the geopolymerization process; with a more significant effect for K_2 sample. The bands at 3430 and 3520cm^{-1}, are clearly distinguishable on the spectrum of K sample, attributable to an elongation vibrations of O-H bond, but tend to disappear on the spectrum of GP, GP_1 and GP_2. Nevertheless, the appearance of the bands around 1400cm^{-1} (Fig. 2c) is related to the vibration of the extended O-C-O bond, reflecting the presence of sodium carbonate in the geopolymer material [10].

In Fig. 2d, the band at 907cm^{-1} on the spectrum of the GP reflects the vibration of elongation of the Al-OH bond, which shifts towards large wave numbers in the spectra of the geopolymers, reflecting media alkalization [19]. Likewise, the bands at 1002 and 1026 cm^{-1} are respectively attributable to the vibrations of symmetrical and asymmetric Si-O-Si bond elongations in kaolinite [20]. These bands decrease in

intensity and move towards large wave numbers, which suggests structural rearrangement within materials following the geopolymerization reaction and the formation of the geopolymer gel [21]. The bands between 3600-3250cm^{-1} and at 1650cm^{-1} are respectively attributable to the vibrations elongation of H-O bond and vibrations deformation of H-O bond in the water molecules absorbed at the surface or present in the cavities of geopolymers [21].

The widening of the bands between 906 and 1025cm^{-1} observed in Fig. 2d for the produced geopolymers confirms that these materials are different from the starting clay samples. Indeed, this broad band can be assigned to the asymmetric elongation vibration of the Si-O and Al-O bonds in the SiO_4 and AlO_4 tetrahedra of geopolymers [22,23].

3.2.2 XRD analysis

Figures 3, 4 and 5 show the XRD patterns of kaolin samples geopolymers. The diffractograms of geopolymers showed the formation of hydroxysodalite as a new crystalline phase. Usually, zeolitic phases are produced during the geopolymerization at elevated temperature [24,25]. It appears that the characteristic peaks of some minerals initially present in the kaolin samples still exist in the XRD patterns of the geopolymer products. These minerals are kaolinite, quartz and gibbsite. However, the decrease of peaks intensity after geopolymerization indicates they remained or partially reacted. Similar observations have been reported by Tchakoute [26]. Indeed, kaolinite has low reactivity in an alkaline medium due to its crystalline structure [27,28].

It should also be noted the appearance of 2 peaks on the XRD patterns of GP_1 and GP_2 at approximately 2θ=76 and 74 respectively. The corresponding minerals those peaks have not been identified yet.

3.2.3 Thermal analysis

Figure 7 shows the thermograms of geopolymers synthetized from raw kaolin and gliding arc plasma treated kaolin in spatial post-discharge mode. These DSC curves highlighted four endothermic phenomena that occur around temperatures of 138, 289, 500 and 770°C. The phenomenon observed at 138°C corresponds to the removal of zeolitic water, while at 289°C, it could be the dehydroxylation of gibbsite for which an alkaline specie did not react with the alkaline activating solution. The most important endothermic phenomenon occurs at 502°C probably corresponding to the elimination of the constitution water of the residual kaolinite contained in the material [18] as indicated by the corresponding FTIR and XRD patterns.

For these two materials of Fig. 7, three exothermic phenomena also occur, in particular temperatures of 40, 852 and 941°C. The exothermic phenomenon observed at 40°C corresponds to the re-initiation of the geopolymerization process of the remaining kaolinite. Considering the fact that the geopolymerization was partial and that the reagents remained in the materials obtained, the gradual increase in temperature during thermal analyses promotes a resumption of the geopolymerization reaction; knowing that the curing temperature improved the geopolymerization process [29]. This geopolymerization process ends

around 852°C but, around 940°C, the structural reorganization of the little metakaolinite formed in spinel occurs.

Figure 7 also shows the thermograms of differential scanning calorimeter (DSC) and thermogravimetric analysis (TGA) which are related to the geopolymer produced from kaolin treated with gliding arc plasma in direct mode (K_1). The DSC curve shows three endothermic phenomena which correspond to temperatures of 92, 142 and 283°C. The phenomenon observed at 92°C would correspond to a structural rearrangement of kaolinite and that at 142°C from zeolitic water while at 283°C, it would be the dehydroxylation of gibbsite. Three exothermic phenomena also occur, particularly at temperatures of 41, 209 and 650°C. The exothermic phenomenon observed at 41°C corresponds to the re-initiation of the geopolymerization process of the remaining kaolinite [29]. This process of geopolymerization is most important and ends around 851°C. Around 650°C, there is an enlargement that could be a consequence of the large thermal gradient in the sample accompanying the continuity of the geopolymerization process during analysis.

3.2.4 BET analysis

As for the about the BET analyses, it emerges from the Table 1 that the geopolymer particles had a larger specific surface area (geopolymers based on raw kaolin: 16.36m^2/g; geopolymers based on treated in direct mode kaolin: 11.67m^2/g; geopolymers based on treated in indirect mode kaolin: 23.67m^2/g) than those of the kaolin samples used (untreated kaolin: 11.06m^2/g; kaolin treated in direct mode: 8.68m^2/g; treated kaolin in indirect mode: 7.14m^2/g) for their production. This increase in the specific surface area is greatly due to the increase in the external surfaces area of the materials synthetized [30,31].

Table 1 Textural properties of GP, GP_1 and GP_2 [16].

Samples	K	GP	K_1	GP_1	K_2	GP_2
BET Surface area (m^2/g)	11.06±0.52	16.36±0.34	8.68±0.35	11.67±0.32	7.14±0.25	23.67±0.37
t-plot Micropore surface area (m^2/g)	5.32	5.40	2.84	4.64	1.38	6.07
t-plot External surface area (m^2/g)	5.73	10.95	5.83	7.03	4.75	17.60
t-plot Micropore volume (cm^3/g)	0.0033	0.0034	0.0019	0.0066	0.0011	0.0012
*BJH desorption average pore diameter (Å)	192.92	127.17	190.50	203.26	169.04	116.48

*BJH: Barrett–Joyner–Halenda.

Figure 8 gives the BET isotherms analyses of the various geopolymers synthetized. From this figure and according to the IUPAC classification, the isotherms were of type IV indicating that the materials synthesized are mesoporous.

In addition, these isotherms contained an H3 type hysteresis loop. This hysteresis manifested itself at the relative pressure value of 0.5. It characterizes the pores between non-rigid aggregates of plate-shaped particles and indicates that the pores in materials are in uniform slit-shaped [32,33].

3.2.5 SEM observations

The samples used for the BET analyses were also used for the SEM and therefore are the ground samples. SEM analyses through Fig. 9, 10 and 11 showing the surface morphology at different scales of the milled geopolymers (Fig. 9 from GP, Fig. 10 from GP_1 and Fig. 11 from GP_2).

As seen in 10 microns scale images of all geopolymer materials, the process of geopolymerization resulted in aggregation of particles. The images obtained at the scale of one micron confirm that the particles have aggregated and they are in the form of plaques. This agrees with the porous slit-shaped network suggested by the type of hysteresis loop (H3 type hysteresis) obtained after the nitrogen physisorption.

3.2.6 Compressive strength

The compression tests depend on the type of kaolin sample used for the synthesis of geopolymer material is shown in Fig. 12. It can be seen that the geopolymer material from the kaolin treated in spatial post-discharge mode had the highest compressive strength (6MPa) while the lowest compressive strength (1.245MPa) were recorded with direct mode treated kaolin based geopolymer. Thus, compared to raw kaolin, the indirect treatment increased the compressive strength of the geopolymer material by 20.48%, while the direct treatment reduces the strength of the geopolymer material by almost 75%. From data of Table 1 in relationship with the micropore volume, we noticed that the compressive strength of the geopolymers was inversely proportional to the pores size within the material. Therefore, the less porous sample had the greatest compressive strength. These observations were in agreement with those reported by Izquierdo et al. [34], demonstrating that increase in porosity affects negatively the mechanical properties of geopolymers.

Also, an increase in the compressive strength of the geopolymer material produced from indirectly treated kaolin may be attributed to an increase in the geopolymerization degree with regards to the greater functionalization (hydroxylation) and the greater hydrophilicity of the kaolin obtained following the treatment in spatial post-discharge mode [15]. Indeed, the high solubility of this sample of kaolin in the alkaline solution may justify fast deconstruction of the aluminosilicate into a reactive precursor ($Si(OH)_4$ and $Al(OH)_4^-$) which could explain the greater geopolymeric reactivity [35]. Further, the compressive strength increases with the extent of geopolymerization [34]. This increase of the compressive strength is in agreement with the results obtained by Xu and Van-Deventer reporting that a greater solubility of aluminosilicates in the alkaline solution is likely to increase the compressive strength of geopolymers [9]. On the other hand, the low strength development for geopolymer derived from directly treated kaolin may would be due to the increase in the degree of crystallinity of kaolinite in that case, which reduced the geopolymeric reactivity. Elimbi et al [11] demonstrated that the decrease in crystallinity of kaolinite promotes the géopolymérisation. As demonstrated in previous work, the high percentage of gibbsite present in raw kaolin as well as its non-reactivity during the geopolymerization process may also contributes to the overall reduction in the compressive strength of the materials produced [26].

4 Conclusion

The results obtained in this work show that using kaolin samples, the geopolymerization process was initiated although it remains unfinished at the curing temperature at which we operated. The geopolymer synthesized from gliding arc plasma treated kaolin in spatial post-discharge mode has the greatest compressive strength representing an improvement rate of 20.48% when compared to the geopolymer based on raw kaolin. On the other hand, a reduction of the compressive strength of 75% is recorded using kaolin treated with gliding arc plasma in direct mode. Thus, the gliding arc plasma treatment of kaolin clay significantly influences its geopolymerization process as well as the compressive strength of the obtained geopolymers. However, these geopolymers have low compressive strength compared to

metakaolin-based geopolymers. For this reason, gliding arc plasma activation of kaolin cannot efficiently replace its heat treatment for geopolymerization process.

Declarations

Acknowledgements

The authors are grateful to Professor Elimbi Antoine of the University of Yaoundé I (Cameroon) for providing clay samples.

Author contributions

B. Sop-Tamo: study conception and design, acquisition of data, analysis and interpretation of data, drafting of manuscript, J.B. Tarkwa: methodology, writing - review & editing, Thamer Alomayri: writing - review & editing, Hasan Assaedi: Writing - review & editing, J. P. Kamseu Mogo: writing - review & editing, J. Baenla: methodology, writing - review & editing, Kamgang-Youbi: writing - review & editing L.N. Tchadjie: methodology, analysis and interpretation of data ,writing - review & editing.

Data availability

All data generated or analysed during this study are included in this article.

Compliance with ethical standards

This manuscript has not been published elsewhere in any form or language and has not been submitted to more than one journal for simultaneous consideration.

Declaration on conflict of interest

The authors declare no conflict of interest.

Code availability

Not applicable

Consent to participate

Not applicable

Consent for publication

Not applicable

Funding statement

Not applicable

References

[1] J. Davidovits, Geopolymers - Inorganic polymeric new materials, J. Therm. Anal. 37 (1991) 1633–1656. doi:10.1007/BF01912193.

[2] R. Abbas, M. Al Khereby, H.Y. Ghorab, N. Elkhoshkhany, Preparation of geopolymer concrete using Egyptian kaolin clay and the study of its environmental effects and economic cost, Clean Technol. Environ. Policy. 22 (2020) 669–687. doi:10.1007/s10098-020-01811-4.

[3] K. Komnitsas, D. Zaharaki, Geopolymerisation : A review and prospects for the minerals industry, Miner. Eng. 20 (2007) 1261–1277. doi:10.1016/j.mineng.2007.07.011.

[4] P. Duxson, A. Fernández-Jiménez, J.L. Provis, G.C. Lukey, A. Palomo, J.S.J. Van Deventer, Geopolymer technology : the current state of the art, J. Mater. Sci. (2007) 2917–2933. doi:10.1007/s10853-006-0637-z.

[5] J. Davidovits, Geopolymer Chemistry and Applications, 3rd ed., Institut Géopolymère, France, 2011.

[6] J.S.J. Van Deventer, J.L. Provis, P. Duxson, G.C. Lukey, Reaction mechanisms in the geopolymeric conversion of inorganic waste to useful products, J. Hazard. Mater. 139 (2007) 506–513. doi:10.1016/j.jhazmat.2006.02.044.

[7] A. Naghizadeh, S.O. Ekolu, Effects of Compositional and Physico – Chemical Mix Design Parameters on Properties of Fly Ash Geopolymer Mortars, Silicon. (2020). doi:10.1007/s12633-020-00799-2.

[8] N. Meftah, M.S. Mahboub, Spectroscopic Characterizations of Sand Dunes Minerals of El-Oued (Northeast Algerian Sahara) by FTIR, XRF and XRD Analyses, Silicon. 12 (2020) 147–153. doi:10.1007/s12633-019-00109-5.

[9] H. Xu, J.S.J. Van Deventer, The geopolymerisation of alumino-silicate minerals, Int. J. Miner. Process. 59 (2000) 247–266. doi:https://doi.org/10.1016/S0301-7516(99)00074-5.

[10] V.F.F. Barbosa, K.J.D. MacKenzie, C. Thaumaturgo, Synthesis and characterisation of materials based on inorganic polymers of alumina and silica: Sodium polysialate polymers, Int. J. Inorg. Mater. 2 (2000) 309–317. doi:10.1016/S1466-6049(00)00041-6.

[11] A. Elimbi, H.K. Tchakoute, D. Njopwouo, Effects of calcination temperature of kaolinite clays on the properties of geopolymer cements, Constr. Build. Mater. 25 (2011) 2805–2812. doi:10.1016/j.conbuildmat.2010.12.055.

[12] C.Y. Heah, H. Kamarudin, A.M. Al Bakri, M. Luqman, I.K. Nizar, Y.M. Liew, Potential Application of Kaolin Without Calcine as Greener Concrete : A Review, Aust. J. Basic Appl. Sci. 5 (2011) 1026–1035.

[13] B. Braggs, J. Ralston, R.S.C. Smart, Surface modification of Kaolinite, WO96/017021, 1996.

[14] H. Ming, K.M. Spark, R.S.C. Smart, Comparison of radio-frequency-plasma- and ion-beam-induced surface modification of kaolinite, J. Phys. Chem. B. 105 (2001) 3196–3203. doi:10.1021/jp0031496.

[15] B. Sop Tamo, G. Kamgang-Youbi, E. Acayanka, L. Medjo Simo, A. Tiya-Djowe, D. Kuete-Saa, S. Laminsi, L. Tchadjie, Plasma Chemical Functionalisation of a Cameroonian Kaolinite Clay for a Greater Hydrophilicity, Plasma Chem. Plasma Process. 36 (2016). doi:10.1007/s11090-016-9731-4.

[16] B. Sop-Tamo, E. Acayanka, W.F. Boyom-Tatchemo, S. Nzali, G. Kamgang-Youbi, S. Laminsi, Gliding arc plasma pre-treatment of kaolin in spatial post-discharge mode for removal of Reactive Red 2 dye from aqueous solution, Water Sci. Technol. 78 (2018) 1448–1458. doi:10.2166/wst.2018.419.

[17] 2005 EN196-1, Methods of testing cement - Part 1: Determination of strength, Eur. Stand. (2005) 1–33.

[18] A.P. Rollet, R. Bouaziz, L'analyse thermique: l'examen du processus chimique, Gauthier-Villars, 1972.

[19] A.B.B. Mohd Mustafa, Y.M. Liew, C.Y. Heah, F.M.T. Muhammad, Clay-Based Materials in Geopolymer Technology, in: Cem. Based Mater., Intech Open, 2018: p. 279. doi:10.5772/intechopen.74438.

[20] A.A.& R.O.O. U.O.Aroke, Fourier-transform infrared characterization of kaolin,Granite,Bentonite and barite, J. Chem. Inf. Model. 53 (2013) 1689–1699. doi:10.1017/CBO9781107415324.004.

[21] Y.M. Liew, H. Kamarudin, A.M. Mustafa Al Bakri, M. Luqman, I. Nizar Khairul, C.Y. Heah, Investigating the possibility of utilization of kaolin and the potential of metakaolin to produce green cement for construction purposes – a review, Aust. J. Basic Appl. Sci. 5 (2011) 441–449.

[22] P. Rovnaník, Effect of curing temperature on the development of hard structure of metakaolin-based geopolymer, Constr. Build. Mater. 24 (2010) 1176–1183. doi:10.1016/j.conbuildmat.2009.12.023.

[23] R.I. Yousef, B. El-eswed, M. Alshaaer, F. Khalili, H. Rahier, Degree of reactivity of two kaolinitic minerals in alkali solution using zeolitic tuff or silica sand filler, Ceram. Int. 38 (2012) 5061–5067. doi:10.1016/j.ceramint.2012.03.008.

[24] E. Prud, P. Michaud, E. Joussein, S. Rossignol, Influence of raw materials and potassium and silicon concentrations on the formation of a zeolite phase in a geopolymer network during thermal treatment, J. Non. Cryst. Solids. 358 (2012) 1908–1916. doi:10.1016/j.jnoncrysol.2012.05.043.

[25] Z. Zheng, X. Ma, Z. Zhang, Y. Li, In-situ transition of amorphous gels to Na-P1 zeolite in geopolymer: Mechanical and adsorption properties, Constr. Build. Mater. 202 (2019) 851–860. doi:10.1016/j.conbuildmat.2019.01.067.

[26] H.K. Tchakoute, C.H. Rüscher, J.N.Y. Djobo, B.B.D. Kenne, D. Njopwouo, Influence of gibbsite and quartz in kaolin on the properties of metakaolin-based geopolymer cements, Appl. Clay Sci. (2015) 1–7. doi:10.1016/j.clay.2015.01.023.

[27] A.D. Hounsi, G.L. Lecomte-nana, G. Djétéli, P. Blanchart, Kaolin-based geopolymers : Effect of mechanical activation and curing process, Constr. Build. Mater. 42 (2013) 105–113. doi:10.1016/j.conbuildmat.2012.12.069.

[28] B.B.D. Kenne, A. Elimbi, M. Cyr, J.D. Manga, H.T. Kouamo, Effect of the rate of calcination of kaolin on the properties of metakaolin-based geopolymers, J. Asian Ceram. Soc. 3 (2015) 130–138. doi:10.1016/j.jascer.2014.12.003.

[29] C.Y. Heah, H. Kamarudin, A.M. Mustafa Al Bakri, M. Binhussain, M. Luqman, I. Khairul Nizar, C.M. Ruzaidi, Y.M. Liew, Effect of curing profile on kaolin-based geopolymers, Phys. Procedia. 22 (2011) 305–311. doi:10.1016/j.phpro.2011.11.048.

[30] J.G.S. Van Jaarsveld, J.S.J. Van Deventer, A. Schwartzman, The potential use of geopolymeric materials to immobilise toxic metals: Part II. Material and leaching characteristics, Miner. Eng. 12 (1999) 75–91. doi:10.1016/S0892-6875(98)00121-6.

[31] J.G.S. Van Jaarsveld, J.S.J. van Deventer, G.C. Lukey, The characterisation of source materials in fly ash-based geopolymers, Mater. Lett. 57 (2003) 1272–1280.

[32] B.D. Adkins, B.H. Davis, Comparison of nitrogen adsorption and mercury penetration results I. Pore volume and surface area obtained for type IV isotherms, Adsorpt. Sci. Technol. 5 (1988) 76–93. doi:10.1177/026361748800500108.

[33] K.S.W. Sing, D.H. Everett, R.A.W. Haul, L. Moscou, R.A. Pierotti, J. Rouquerol, T. Siemieniewska, Reporting physisorption data for gas / solid systems with special reference to the determination of surface area and porosity (recommendations 1984), Pure Appl. Chem. 57 (1985) 603–619.

[34] Y. Luna-Galiano, C. Fernández-Pereira, M. Izquierdo, Contributions to the study of porosity in fly ash-based geopolymers . Relationship between degree of reaction , porosity and compressive strength, Mater. Construcción. 66 (2016) e098. doi:10.3989/mc.2016.10215.

[35] X. Yao, Z. Zhang, H. Zhu, Y. Chen, Geopolymerization process of alkali – metakaolinite characterized by isothermal calorimetry, Thermochim. Acta. 493 (2009) 49–54. doi:10.1016/j.tca.2009.04.002.

Figures

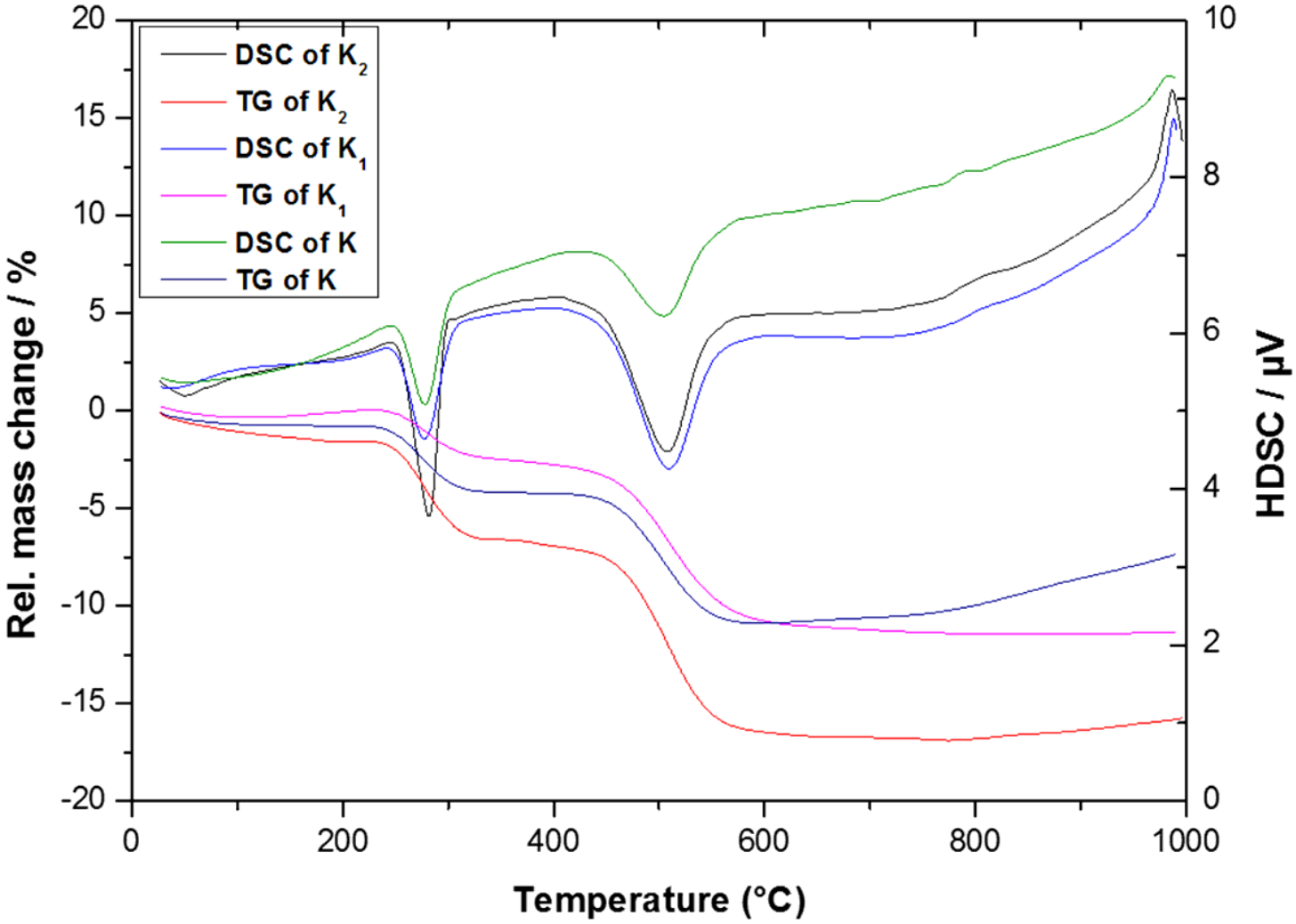

Figure 1

DSC and TGA thermograms of kaolin samples (K, K1 and K2).

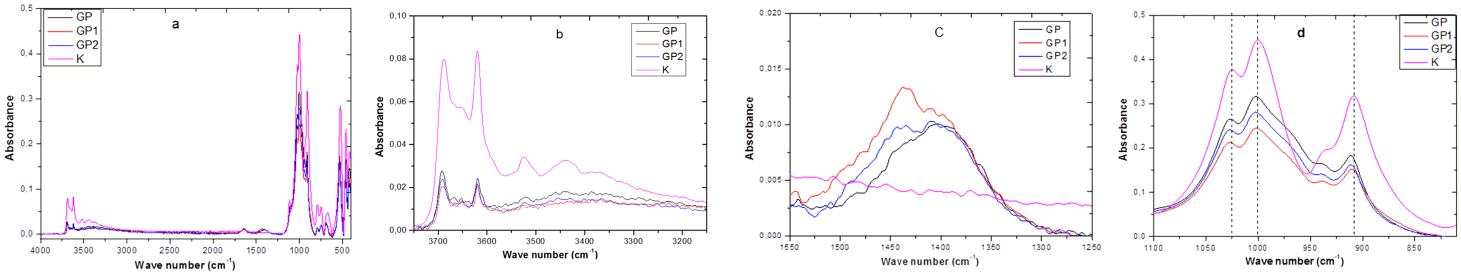

Figure 2

a FTIR spectra of K, GP, GP1 and GP2. b Zoom in on the spectra in Fig. 2a in the wavenumber range of 3150 to 3750 cm-1. c Zoom in on the spectra in Fig. 2a in the wavenumber range of 1250 to 1550 cm-1. d Zoom in on the spectra in Fig. 2a in the wavenumber range of 810 to 1100 cm-1.

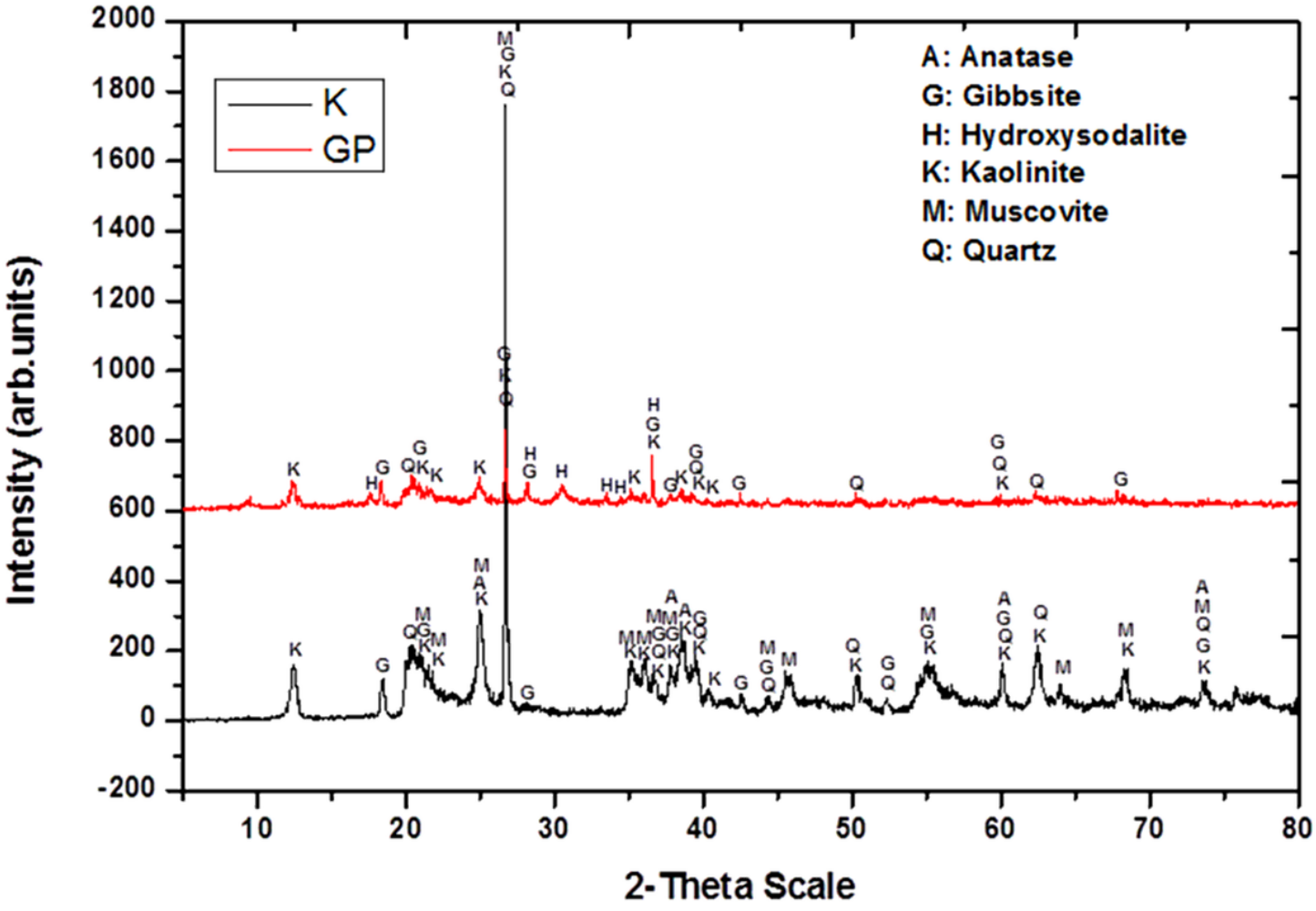

Figure 3

XRD patterns of K and GP.

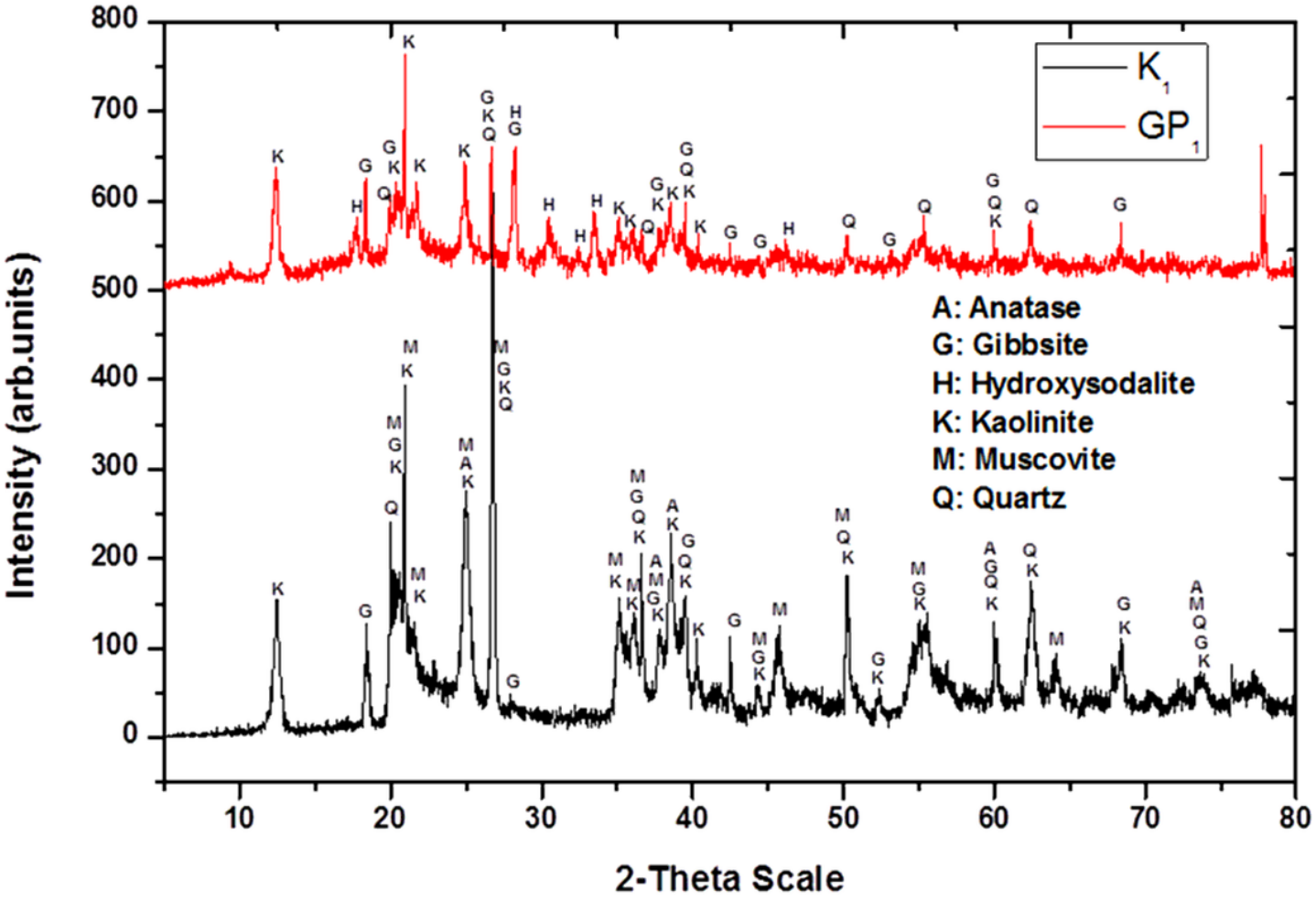

Figure 4

XRD patterns of K1 and GP1.

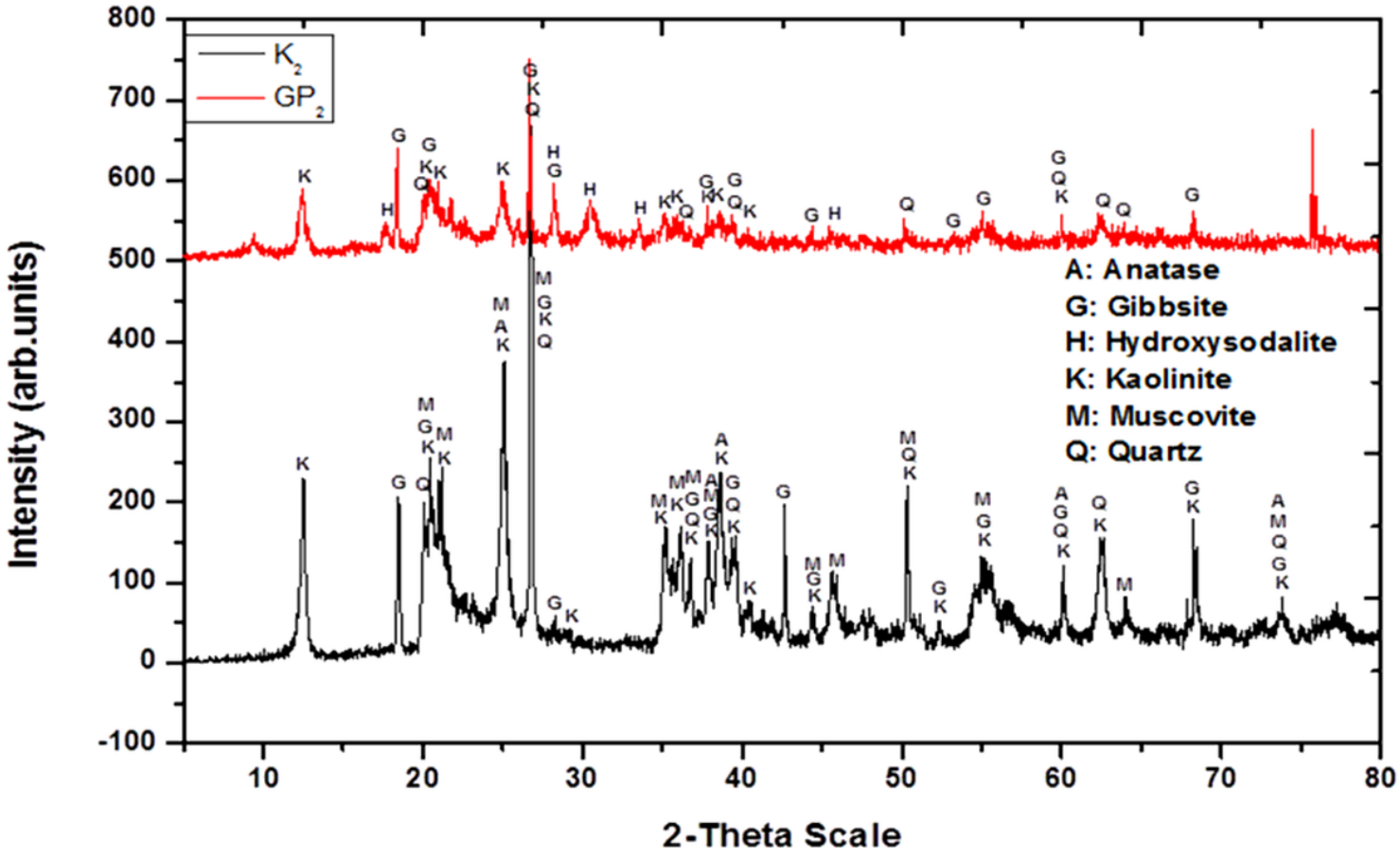

Figure 5

XRD patterns of K2 and GP2.

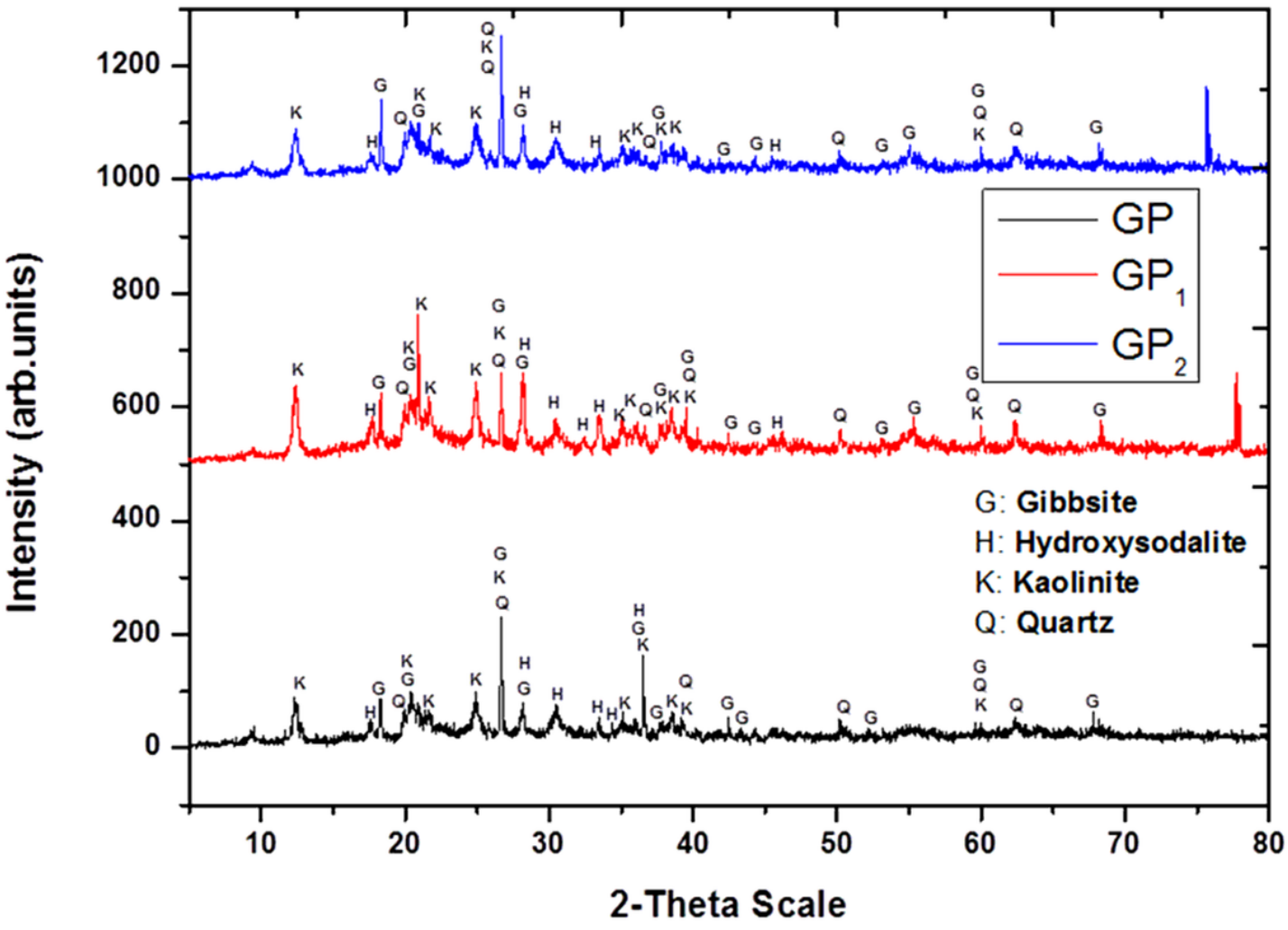

Figure 6

XRD patterns of the different produced materials.

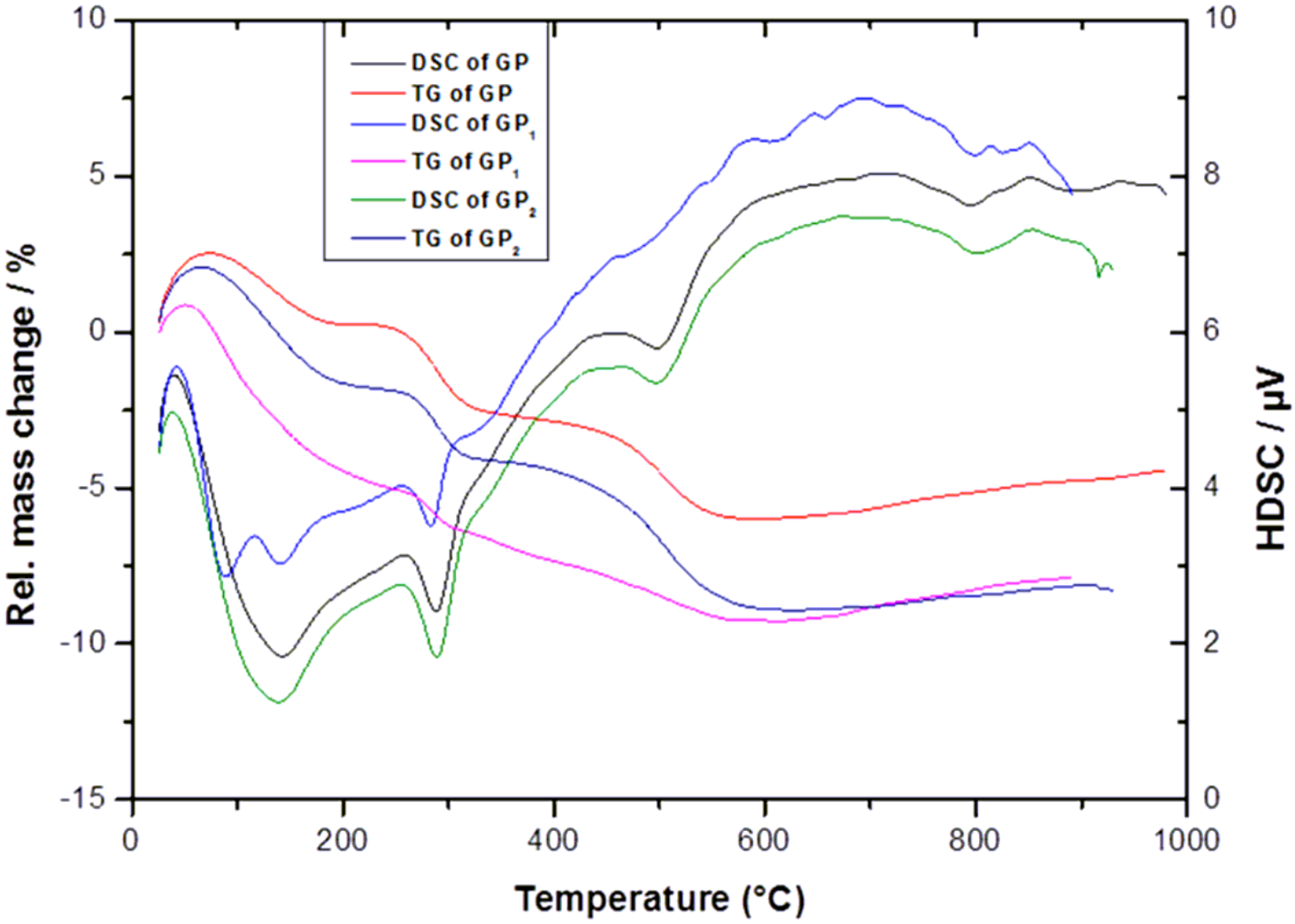

Figure 7

DSC and TGA thermograms of the geopolymers (GP, GP1 and GP2).

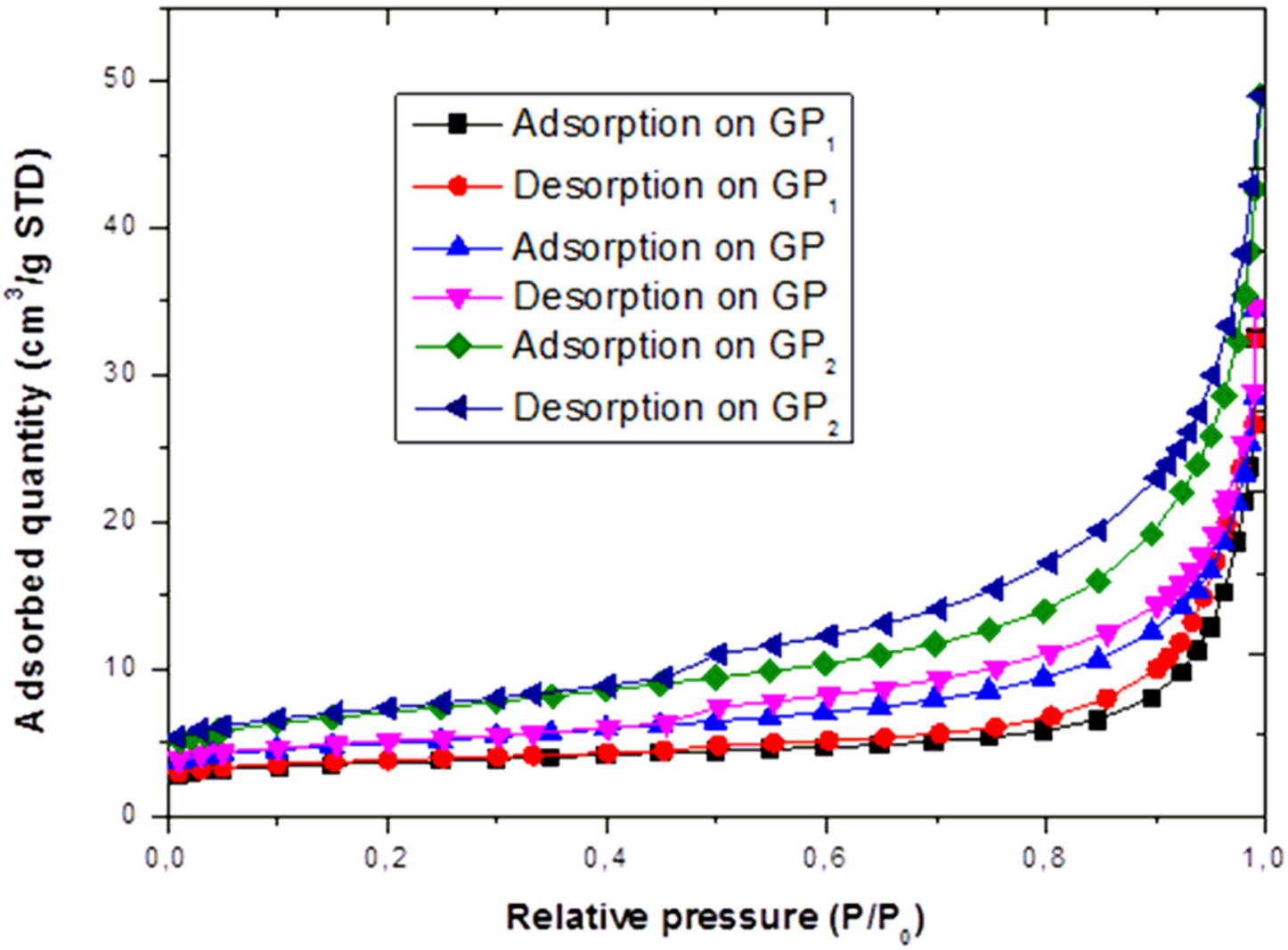

Figure 8

BET isotherms analyses of the various synthetized geopolymers.

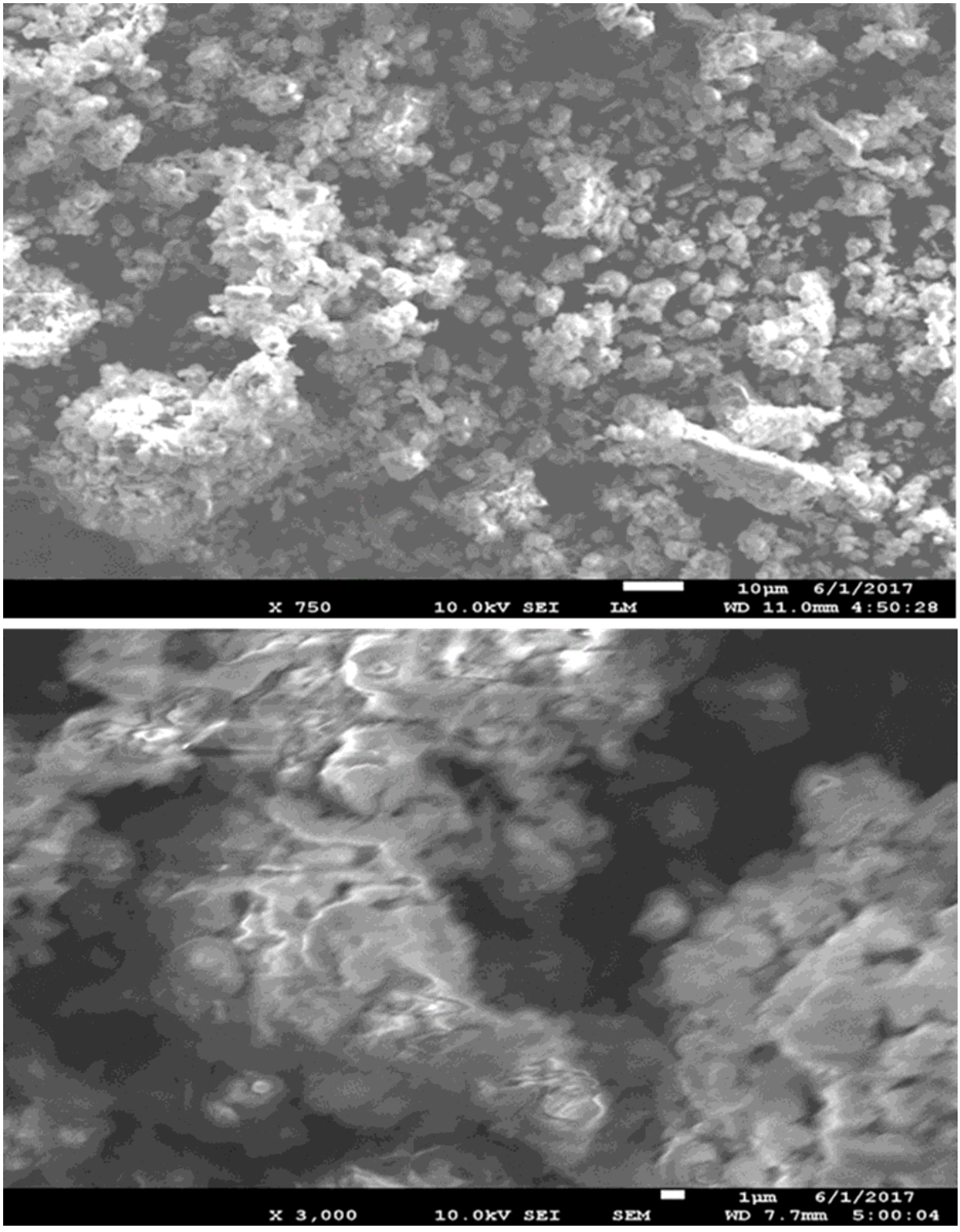

Figure 9

SEM of GP.

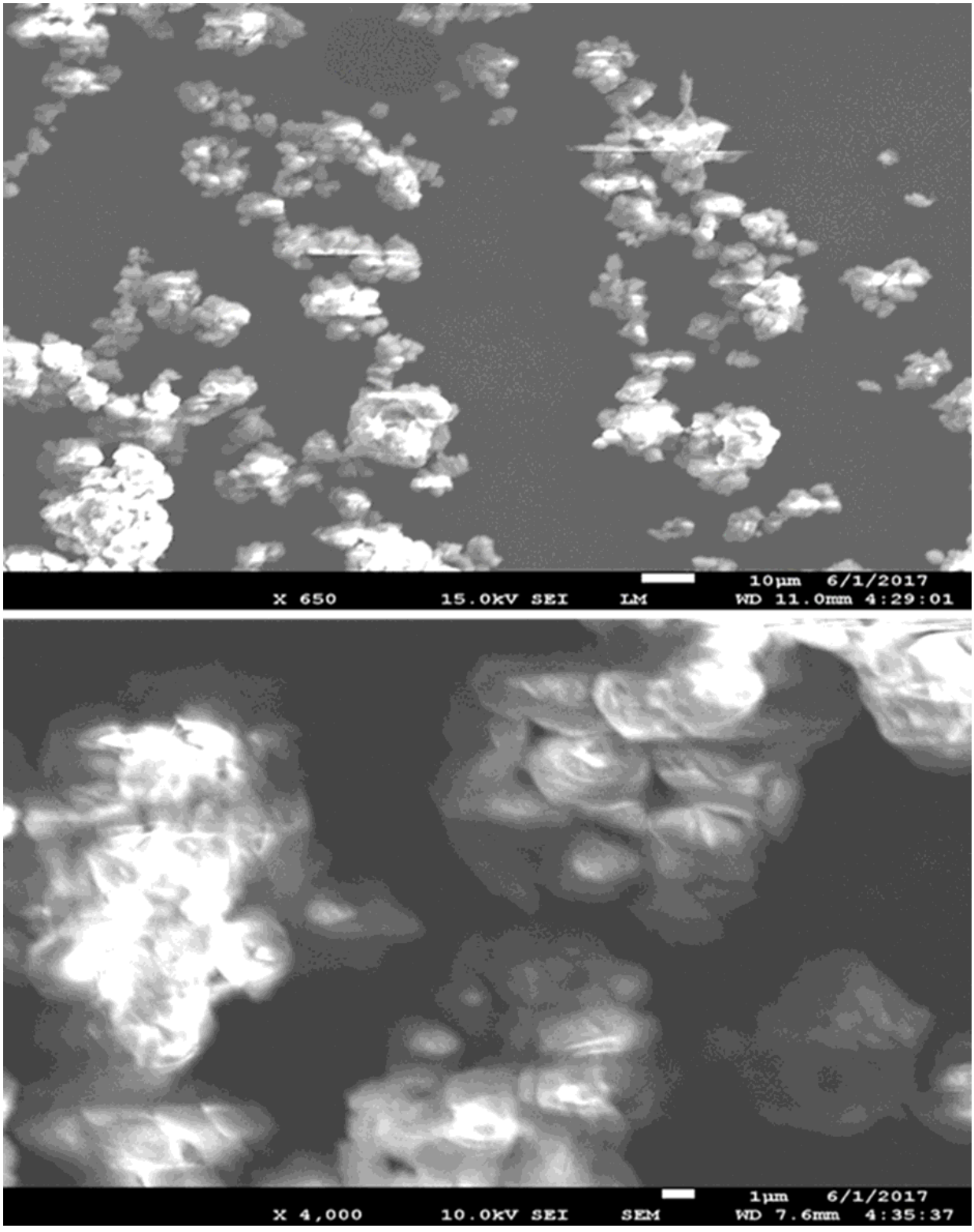

Figure 10

SEM of GP1.

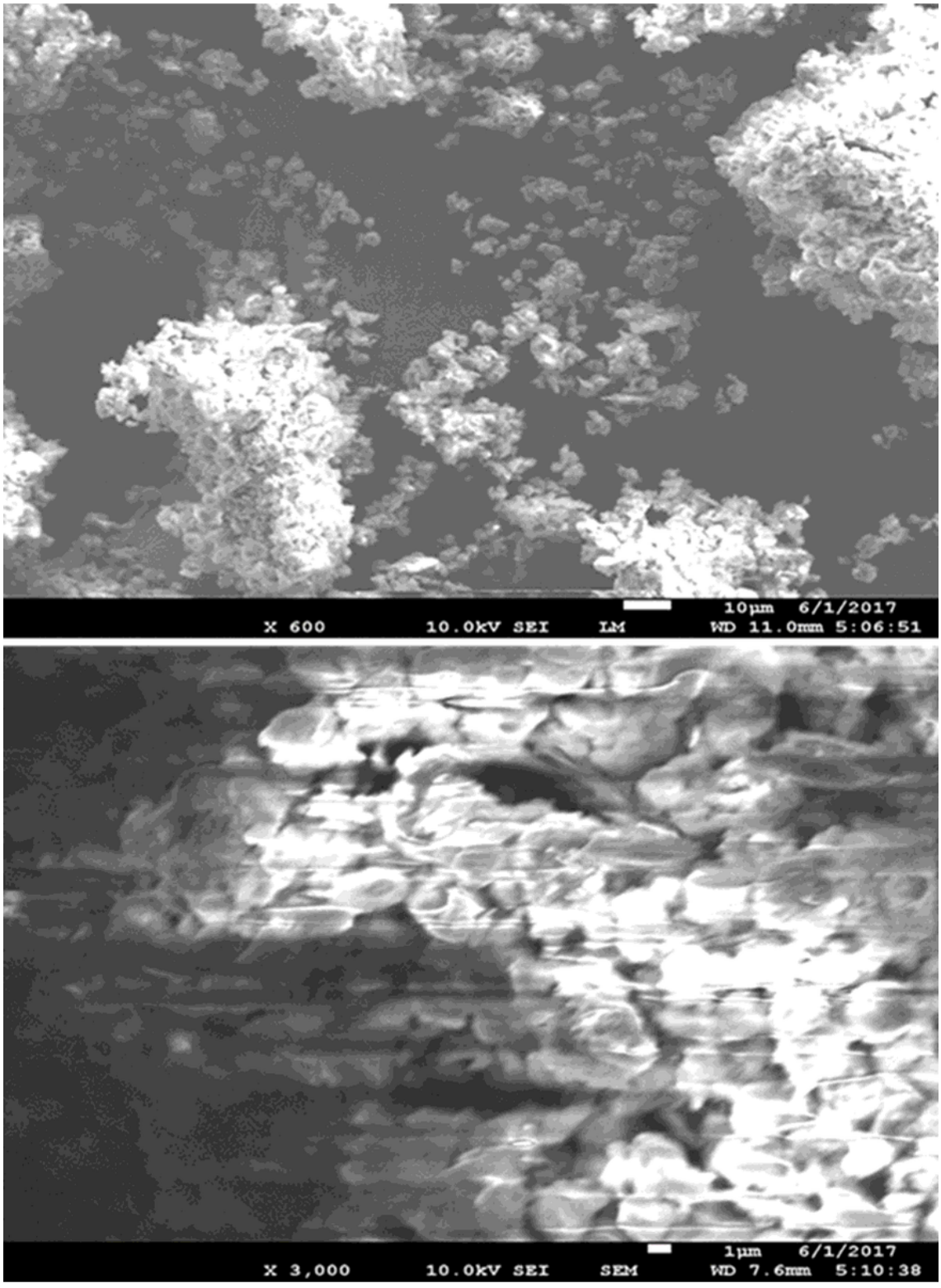

Figure 11

SEM of GP2.

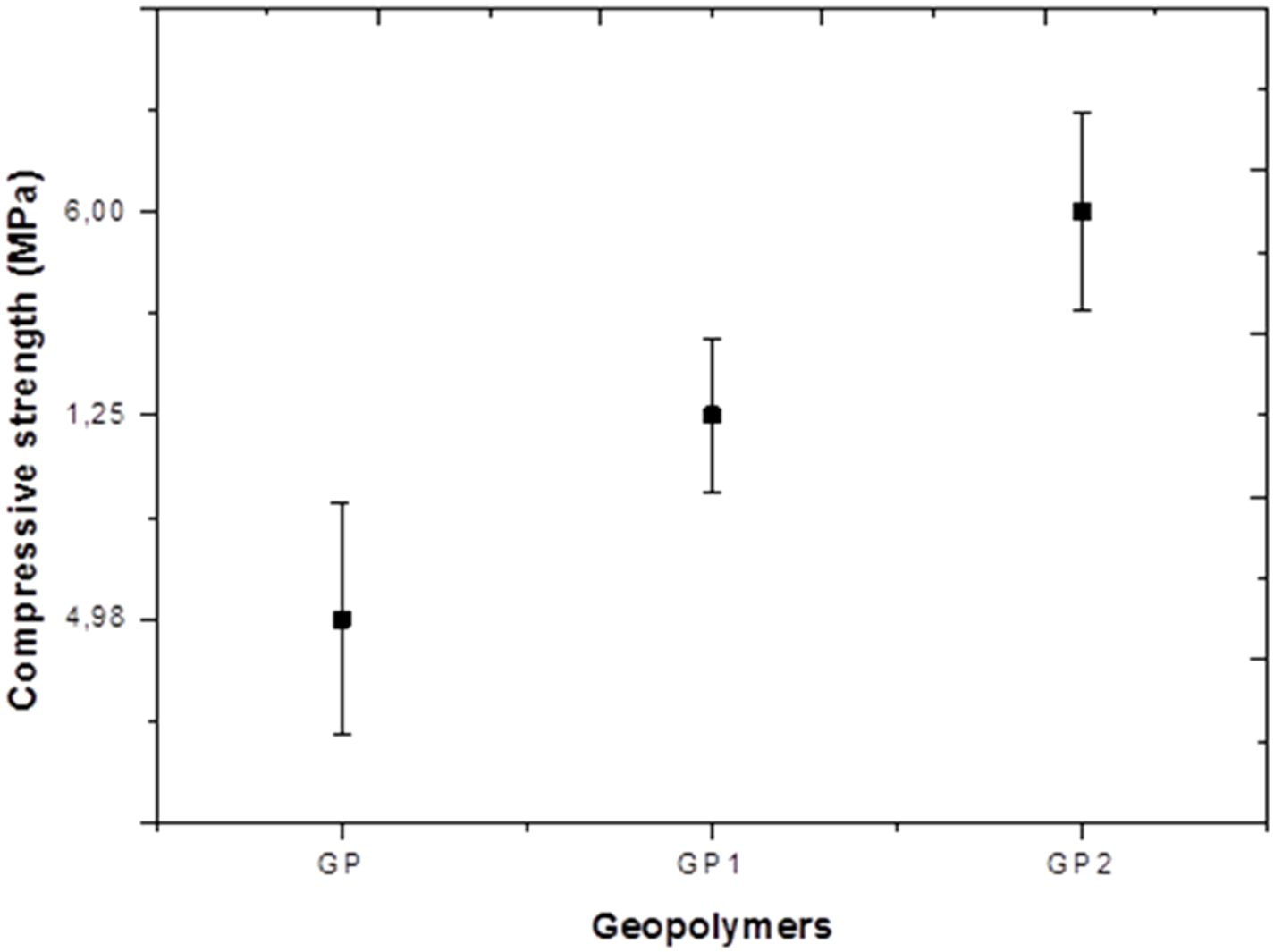

Figure 12

Compressive strengths of GP, GP1 and GP2.